Approach for simultaneous measurement of two-dimensional angular distribution of charged particles. II. Deceleration and focusing of wide-angle beams using a curved mesh lens

Hiroyuki Matsuda and Hiroshi Daimon

Graduate School of Materials Science, Nara Institute of Science and Technology (NAIST), 8916-5 Takayama, Ikoma, Nara 630-0192, Japan and CREST, Japan Science and Technology Agency (JST), 4-1-8 Honcho, Kawaguchi, Saitama 332-0012, Japan

(Received 13 April 2006; published 5 September 2006)

Recently, it was shown that using an ellipsoidal mesh in an einzel-type lens, spherical aberration can be corrected over a wide acceptance angle of up to 120°. The present paper creates the possibility for beam analysis by achieving dramatic improvements in deceleration lens capabilities. This provides a scheme for simultaneous angular distribution measurement suitable for application to high-energy charged-particle beams up to around 10 keV. We consider the behavior of wide-angle charged-particle beams in electrostatic fields given by simple solutions of the Laplace equation, starting with a discussion on a spherically symmetric deceleration field. A beam focusing over a wide acceptance angle of 100° is found in a special spherically symmetric field. However, in many cases of the spherically symmetric field, focusing of wide-angle beams is obstructed by the presence of spherical aberration. We show that the spherical aberration can be corrected by two kinds of deformation of the spherically symmetric field, a deformation of the field under a spherical boundary condition and an ellipsoidal deformation of the field. We study practical realization of such fields under the use of a few electrodes and a curved mesh (spherical or ellipsoidal mesh). Some variations of the arrangement of electrodes are considered, and simple designs of deceleration lenses with wide acceptance angles of up to 120° are obtained. Here fine focusing of wide-angle beams can be achieved in a three-electrode deceleration lens with an ellipsoidal mesh.

DOI: 10.1103/PhysRevE.74.036501 PACS number(s): 41.85.Gy, 41.85.Ne, 87.64.Lg

I. INTRODUCTION

Realization of wide acceptance angles in electron lenses, allowing simultaneous measurement of two-dimensional angular distribution of charged particles, is of great fascination for surface and materials analysis techniques such as x-ray photoelectron spectroscopy (XPS). Its achievement has been obstructed by the problem of spherical aberration. Instead, a mirror optical technique (the display-type spherical mirror analyzer) being free of this problem has been developed [1–4], which served for determination of the Fermi surface and band structure in two dimensions (2D) or three dimensions (3D) [5–8] and for direct recognition of 3D atomic arrangement (stereo atomscopy) [9–11]. Recently, however, based on the use of meshes [12–14], remarkable progress has been made in the correction of spherical aberration [15]. It was shown that it is possible, using an ellipsoidal mesh in an einzel-type lens, to correct spherical aberration over a wide acceptance angle of up to 120° (±60°). The proposed lens is the combination of two opposite fields in close proximity to each other, similar to the well-known combination of concave and convex lenses in light optics. The principle of the correction in this lens is that the field around a mesh generates negative spherical aberration in the virtual image plane and compensates positive spherical aberration of a focusing field. The mesh lens can be used as an objective lens to provide powerful analysis capabilities for, e.g., electronic structure analysis, photoelectron diffraction, stereo atomscopy, and depth profile based on angle-resolved spectroscopy.

The purpose of this paper is to provide a scheme for simultaneous angular distribution measurements suitable for application to high-energy charged-particle beams up to around 10 keV. In recent high-energy XPS [16–21], photon energies up to around 10 keV are used for excitation of inner-core electrons or to obtain bulk or interface information utilizing a long sampling depth. Notice that the wide-angle mesh lens in Ref. [15] produces an output beam with the same kinetic energy as the initial beam. This condition would not be practically convenient for high-energy XPS and related techniques. In general, it is difficult to focus high-energy charged-particle beams (under a conventional lens condition) unless the beam divergence angle is considerably small around a few degrees. For simultaneous angular distribution measurements in the case of high-energy charged-particle beams up to around 10 keV, it is desired that an objective lens not only focus a wide-angle beam, but also, simultaneously, reduce the kinetic energy of the beam. However, deceleration lenses, in general, have a great disadvantage in the collection and focusing of charged particles. The present paper, therefore, tries to achieve dramatic improvements in deceleration lens capabilities.

We consider the behavior of wide-angle charged-particle beams in deceleration fields given by simple solutions of Laplace equation. We start with showing the beam behavior in a spherically symmetric field between two concentric spheres (in a situation where charged particles enter the field from the inner boundary) and then consider deformation of the field to correct spherical aberration. A similar analysis was performed in Refs. [14,15] under the consideration of virtual images. The present paper examines the possibility of focusing wide-angle beams without the use of a focusing field of acceleration, such as in Refs. [14,15]. The beam behavior in the spherically symmetric field is discussed using the exact solution of the equation of motion [1,2]. We take into account two essentially different deformations of the

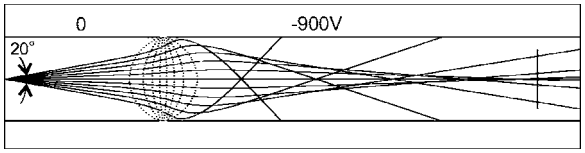

FIG. 1. Spherical aberration of a typical cylindrical deceleration lens. Electron trajectories with initial angles up to ±10 are shown. The initial energy of the electrons is 1 keV and a voltage of −900 V is applied to the second electrode. The bar in the exit region marks the Gaussian image plane.

spherically symmetric field; a deformation of the field under a spherical boundary condition, which is considered in the same manner as in Ref. [14], and an ellipsoidal deformation of the field, which is considered using a simple solution of the Laplace equation in a prolate spheroidal coordinate system. These deformations will be shown to be responsible for deceleration and focusing of wide-angle beams. After these considerations, we will proceed to the practical design of wide-angle deceleration lenses.

In Sec. II, our basic consideration based on simple solutions of Laplace equation is given. In Sec. III, practical lens design is studied under the use of a spherical mesh and a few electrodes, taking into account appropriate electrode arrangements. In Sec. IV, we consider three-electrode deceleration lenses with an ellipsoidal mesh. Here, beam focusing over wide acceptance angles up to 120° is realized. Sec. V is devoted to discussion and conclusion.

II. THEORETICAL CONSIDERATIONS USING SIMPLE SOLUTIONS OF THE LAPLACE EQUATION

Ordinary electron lenses yield large spherical aberration for rays passing through a region far from the optical axis. In general, deceleration lenses (while responsible for providing better energy resolution) are not suited for beam focusing, because they have a local divergent field at the entrance side. An example of ray tracing in a deceleration lens is shown in Fig. 1. Here a large spherical aberration is produced even for small initial angles of around ±5°. Thus, beam focusing in ordinary deceleration lenses requires that the beam divergence angle be limited to a considerably small degree. In

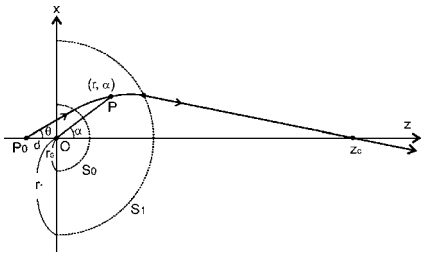

FIG. 2. Use of a spherically symmetric field (Coulomb field) as a lens. The field is given in the region between two half-spherical surfaces S_0 and S_1, and the other region (including the electron source P_0) is set to be field free. The electron position P is specified in polar coordinates (r,α). An electron, starting from the source P_0, is bent by the field and crosses the optical axis at $z=z_c$.

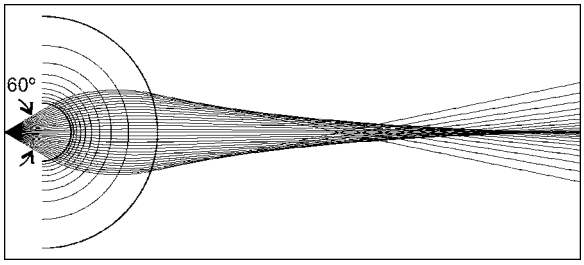

FIG. 3. Electron trajectories in the spherically symmetric field for $E_f/E_i=0.1$, $r_1/r_0=4$, and $d/r_0=1.72$. Initial angles up to ±30° are considered.

Secs. II A–II C basic considerations using simple solutions of Laplace equations are presented to dramatically increase acceptance angles of deceleration lenses.

A. Spherical aberration in a spherically symmetric field

Let us first discuss spherical aberration behavior in a spherically symmetric field. We consider the situation depicted in Fig. 2. A spherically symmetric field is given in the region between two half-spherical surfaces S_0 and S_1. Here the region inside S_0 and outside S_1 is set to be field free. The potential function $\Phi(r)$ for the field with the condition $\Phi(r_0)=0$ is given by

$$\Phi(r)=\frac{r_1 V}{r_1-r_0}\left(1-\frac{r_0}{r}\right), \tag{1}$$

where r_0 and r_1 are the radii of S_0 and S_1, respectively, and V is the potential difference between S_1 and S_0. The electron source P_0 is at a distance d from the center O of the spheres. An electron, starting from P_0 with an initial angle θ and decelerated in the field between S_0 and S_1, crosses the optical axis z in the region outside S_1 for some range of the initial energy E_i of the electron.

Taking polar coordinates (r,α) at O, the solution for the electron trajectory in the region between S_0 and S_1 (see Refs. [1,2]) is given by

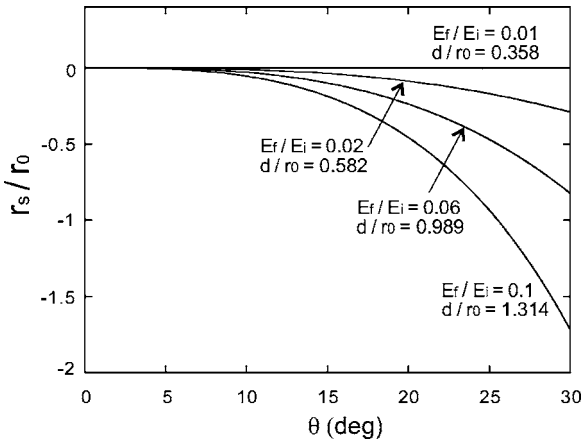

FIG. 4. Spherical aberration of the spherically symmetric field for various E_f/E_i and d/r_0. In the case E_f/E_i=from 0.1 to 0.02, the ratio r_1/r_0 is fixed at 4. In the case $E_f/E_i=0.01$, r_1/r_0 is adjusted to obtain fine focusing.

$$r = \frac{(d^2/r_0)\,\eta \sin^2\theta}{1 - \xi \sin\alpha \sin\beta - \xi \cos\alpha \cos\beta}, \tag{2}$$

where

$$\eta = E_i/E_0, \quad E_0 = \frac{r_1 eV}{2(r_1 - r_0)}, \tag{3}$$

$$\xi = [1 + \eta(\eta - 2)(d^2/r_0^2)\sin^2\theta]^{1/2}, \tag{4}$$

$$\beta = \theta - \omega, \quad \tan\omega = \frac{(\eta - 1)d\sin\theta}{\sqrt{r_0^2 - d^2\sin^2\theta}}. \tag{5}$$

(e is the elementary charge and E_0 is the energy of an electron undergoing circular motion at $r=r_0$.) For a given $r(r_0 \leqslant r \leqslant r_1)$, the electron position P in Fig. 2 is determined by

$$\cos\alpha = \frac{\zeta(r)\cos\beta - \sin\beta\sqrt{\xi^2 - \zeta(r)^2}}{\xi}, \tag{6}$$

where

$$\zeta(r) = 1 - \frac{\eta d^2}{r_0 r}\sin^2\theta. \tag{7}$$

The condition $\xi^2 - \zeta(r)^2 \geqslant 0$ means that the electron passes or reaches the spherical surface of radius r. Taking $r=r_1$, it holds when

$$\eta \geqslant \frac{2(1 - r_0/r_1)}{1 - (d^2/r_1^2)\sin^2\theta} > 2\left(1 - \frac{r_0}{r_1}\right). \tag{8}$$

The axially crossing position z_c is given by

$$z_c = z_1 - x_1 \left.\frac{\partial z}{\partial x}\right|_{r=r_1}, \tag{9}$$

where (z_1, x_1) denotes the z, x coordinate point of the electron at the surface of $r=r_1$. Real images are obtained when the slope $\left.\frac{\partial z}{\partial x}\right|_{r=r_1}$ of the trajectory at $r=r_1$ is negative. (For $\left.\frac{\partial z}{\partial x}\right|_{r=r_1} > 0$, Eq. (9) gives the axially crossing position at the virtual image.) The slope is given by

$$\left.\frac{\partial z}{\partial x}\right|_{r=r_1} = -\frac{[\zeta(r_1) - \xi^2]\sin\beta + \cos\beta\sqrt{\xi^2 - \zeta(r_1)^2}}{[\zeta(r_1) - \xi^2]\cos\beta - \sin\beta\sqrt{\xi^2 - \zeta(r_1)^2}}. \tag{10}$$

Inserting the solution for (z_1, x_1) and Eq. (10) into Eq. (9), we obtain

$$z_c = \frac{(d^2/r_0)\,\eta\xi\sin^2\theta}{[\zeta(r_1) - \xi^2]\cos\beta - \sin\beta\sqrt{\xi^2 - \zeta(r_1)^2}}. \tag{11}$$

The position of the Gaussian image plane (z_c at $\theta \to 0$) is given by

$$z_G = \frac{\eta r_1}{-\eta - \eta(\eta - 2)\dfrac{r_1}{r_0} - \left[\dfrac{r_1}{d} - (\eta - 1)\dfrac{r_1}{r_0}\right]\sqrt{\eta(\eta - 2) + 2\eta\dfrac{r_0}{r_1}}}. \tag{12}$$

Taking into account the limit $d \to \infty$ in Eq. (12), it can be seen that the condition for $z_G > 0$ satisfies

$$\eta < \frac{2}{1 + r_0/r_1}. \tag{13}$$

The beam behavior in the spherically symmetric field is determined by the parameters η, d/r_0, and r_1/r_0. The ratio E_f/E_i of the final kinetic energy to the initial one, i.e., the deceleration ratio is given by $E_f/E_i = 1 - eV/E_i = 1 - 2(r_1 - r_0)/r_1\eta$. The spherical aberration is largely dependent on the electron source position. Large spherical aberration is produced in the case where the electron source is at a relatively large distance from the entrance of the field. An example is given in Fig. 3, where electron trajectories with initial angles up to $\pm 30^\circ$ are shown. The deceleration ratio E_f/E_i is 0.1, the same as in Fig. 1. The spherical aberration is much smaller than that of an ordinary deceleration lens, as seen from the comparison with Fig. 1. In Fig. 4, it is shown that the spherical aberration can be greatly reduced by choosing a smaller value of d/r_0. In this case, to produce a real image with better focusing, a higher deceleration voltage should be applied to the outer boundary surface. In this way, fine focusing of wide-angle beams can be achieved in the spherically symmetric field. A remarkable example is shown in Fig. 5, where focusing over a wide divergence angle of 100° is realized by choosing $E_f/E_i = 0.01$, $d/r_0 = 0.511$, and $r_1/r_0 = 5.56$.

A high deceleration value of around $E_f/E_i = 0.01$ may be appropriate for beams with high energies around 10 keV. However, a reasonable choice of E_f/E_i to cover a wide energy range from below 1 keV to around 10 keV is rather around 0.1. In this case, it is required that spherical aberration be corrected in a certain way, which is considered in Secs. II B and II C.

B. Spherical aberration correction by field deformation under a spherical boundary condition

Consider a deformation of the spherically symmetric field under the spherical boundary condition that $\Phi = 0$ for $r=r_0$, irrespective of α. The rotational symmetry with respect to

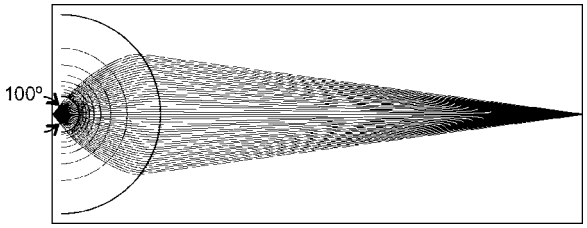

FIG. 5. Electron trajectories in the spherically symmetric field for $E_f/E_i=0.01$, $r_1/r_0=5.56$, and $d/r_0=0.511$. Initial angles up to ±50° are considered.

the optical axis is also imposed. The general solution of the Laplace equation under these conditions can be expressed in a series of spherical harmonics as $\Sigma_{n=0}^{\infty}A_n(r^n - r_0^{2n+1}/r^{n+1})P_n(\cos\alpha)$, with arbitrary constants A_n (P_n represents Legendre polynomials) [14]. The spherically symmetric potential (1) is given by the term of $n=0$. We consider only the term of $n=1$ for deformation of the spherically symmetric field, i.e., consider the following solution:

$$\Phi(r,\alpha) = A_0\left(1 - \frac{r_0}{r}\right) + A_1\left(r - \frac{r_0^3}{r^2}\right)\cos\alpha. \tag{14}$$

In Ref. [14], the solution with the terms of $n=0$, $n=1$, and $n=2$ was considered, and then beam focusing over a large acceptance angle of 60° was shown to be possible by regulating A_0, A_1, and A_2; the term of $n=2$ was set to give a focusing field of acceleration. We consider beam focusing without the use of such a focusing field.

Starting from the case of Fig. 3 (the spherically symmetric case $A_1=0$), the spherical aberration can be reduced by increasing the contribution of the second term in Eq. (14) with $A_1/A_0>0$. For fine correction of spherical aberration, it is required to optimize the possible parameters A_0, A_1, and d. An example of the optimization is given in Fig. 6(a). Here

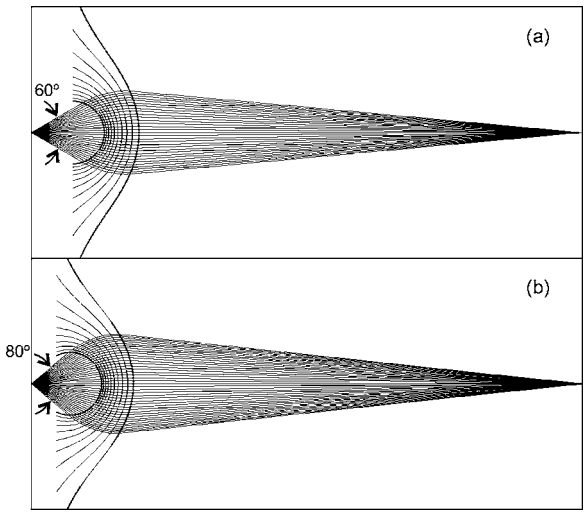

FIG. 6. Results of optimization in the deformation of the spherically symmetric field under a spherical boundary condition for acceptance angles of (a) 60° and (b) 80°. Electron trajectories with initial angles up to (a) ±30° and (b) ±40° are shown. The deceleration ratio E_f/E_i is 0.1.

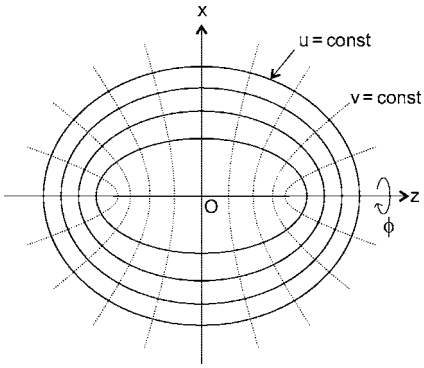

FIG. 7. Illustration of a prolate spheroidal coordinate system (u,v,ϕ). Shown are u-constant and v-constant curves in the z,x plane. The azimuth ϕ refers to the rotation of coordinate points around the z axis.

spherical aberration is finely corrected over a large acceptance angle of 60°. When using a spherical boundary surface larger than half of a sphere, it is possible to correct spherical aberration over larger acceptance angles up to around 80°, as shown in Fig. 6(b). Figure 6 gives the possibility of realizing wide-angle deceleration lenses using a spherical mesh (for practical lens design, see Sec. III).

C. Spherical aberration correction by ellipsoidal field deformation

Next, we show that an ellipsoidal deformation of the spherically symmetric field enables correction of spherical aberration over larger acceptance angles. Consider ellipsoidal coordinates (u,v,ϕ) shown in Fig. 7 [a prolate spheroidal coordinate system (see, e.g., Refs. [22,23]) with foci on the optical axis z]. Here ϕ is the azimuthal angle with respect to the z axis. Let f be the focal distance from O, i.e., foci at $z=\pm f$. Then the coordinates u, v, and ϕ are connected with the rectangular coordinate system by

$$x = f\sqrt{u^2-1}\sqrt{1-v^2}\cos\phi, \tag{15}$$

$$y = f\sqrt{u^2-1}\sqrt{1-v^2}\sin\phi, \tag{16}$$

$$z = fuv, \tag{17}$$

with permissible ranges $1\leqslant u<\infty$, $-1\leqslant v\leqslant 1$, and $0\leqslant\phi\leqslant 2\pi$. It is easily seen that Eqs. (15)–(17) satisfy the ellipsoid equation $z^2/(fu)^2+(x^2+y^2)/[f^2(u^2-1)]=1$. Thus, for a given u, the variables v and ϕ give a confocal ellipsoid with a major radius of fu and a minor radius of $f\sqrt{u^2-1}$. In this coordinate system, an ellipsoidal boundary condition that $\Phi=0$ for $u=u_0$, irrespective of (v,ϕ), can be well introduced into the solution Φ of the Laplace equation. A simple solution is given by

$$\Phi(u) = A\ln\frac{u-1}{u+1} - A\ln\frac{u_0-1}{u_0+1}, \tag{18}$$

where A is an arbitrary constant. It is useful to express A by

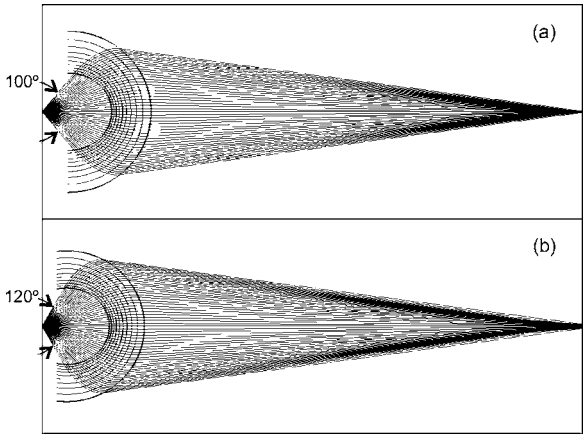

FIG. 8. Results of optimization in the ellipsoidal deformation of the spherically symmetric field. Electron trajectories with initial angles up to (a) ±50° and (b) ±60° are shown. The ratio γ of the two radii of the boundary ellipsoid of $u=u_0$ is both around $\gamma=1.12$. The deceleration ratio E_f/E_i is 0.1.

$$A = V \Big/ \ln\left(\frac{u_1 - 1}{u_1 + 1}\frac{u_0 + 1}{u_0 - 1}\right), \tag{19}$$

where $V=\Phi(u_1)$. It is easy to verify that in the limit $f\to 0$, Eq. (18), together with Eq. (19), leads to Eq. (1) when setting $r_0=fu_0$, $r_1=fu_1$, and $r=fu$.

In the present case, spherical aberration can be reduced by increasing the ratio $\gamma=u_0/\sqrt{u_0^2-1}$ of the two radii of the boundary ellipsoid of $u=u_0$, starting from the spherically symmetric case $\gamma=1$. Figure 8 shows results of optimization in this approach. In Fig. 8(a), spherical aberration is well corrected over a wide acceptance angle of 100°. Figure 8(b) suggests that spherical aberration can be corrected over wider acceptance angles up to around 120° by using a boundary surface larger than half of an ellipsoid. The values of the ellipsoidal shape parameter γ obtained for the two cases are both around $\gamma=1.12$. Thus beam deceleration and focusing over a wide acceptance angle can be achieved by a small deformation of the spherically symmetric field. It should be noted, however, that the fields in Fig. 8 have two ellipsoidal boundaries, which requires the use of two ellipsoidal meshes for actual realization. In Sec. IV we try to achieve deceleration and focusing of wide-angle beams with the use of a single ellipsoidal mesh.

III. DECELERATION AND FOCUSING OF WIDE-ANGLE BEAMS USING A SPHERICAL MESH

Here and in the following section, we consider practical realization of wide-angle deceleration lenses. This section studies the possibility of the use of a spherical mesh, following Sec. II B. Let us first consider an equidiameter two-cylinder lens with a spherical mesh. In Fig. 9(a), we show a design of the lens with an acceptance angle of 40° (±20°). Here spherical aberration is well corrected over the acceptance angle. The mesh is given to the front electrode EL1, which is set at ground potential. A decelerating voltage V_2 is applied to the rear electrode EL2. When the initial electron energy is 1 keV, the voltage V_2 is set to −835 V; the deceleration ratio is 0.165.

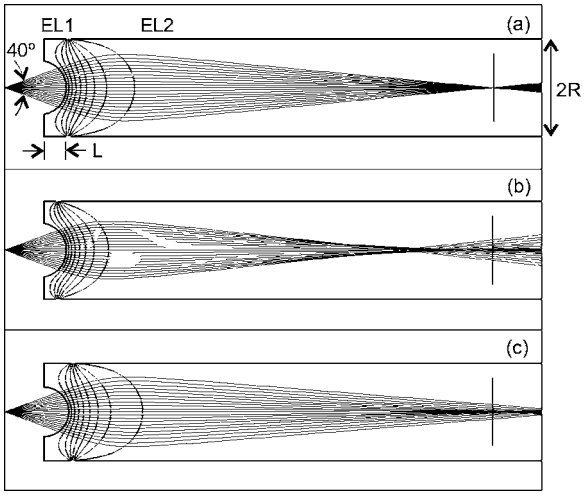

FIG. 9. Equidiameter two-cylinder lens with a spherical mesh. Three different conditions are considered: (a) $L/R=0.448$, (b) $L/R=0.24$, and (c) $L/R=0.54$. Equipotential lines and electron trajectories with initial angles up to ±20° are shown. The bar in the focusing region marks the Gaussian image plane. The condition (a) provides beam focusing at the image plane. In the conditions (b) and (c), positive and negative spherical aberrations are produced, respectively.

There are some parameters that determine the aberration behavior of the lens. An important parameter is the length L of the front electrode [see Fig. 9(a)]. This parameter allows us to effectively control the electrostatic field around the mesh. Increasing L (decreasing L) results in a shift of the image position z to larger z (smaller z). In Figs. 9(b) and 9(c), opposite variations from Fig. 9(a) are considered, with V_2 set to give the Gaussian image plane at the same position. As seen here, the parameter L allows reversing the sign of the aberration; positive and negative spherical aberrations are generated in Figs. 9(b) and 9(c), respectively. Figure 10 shows the spherical aberration behavior of the lens for some variations of L. The spherical aberration becomes very small at certain L, around which the sign of the aberration changes.

It is remarkable that such a simple lens design as in Fig. 9 gives a considerable improvement of an ordinary deceleration lens. A further improvement of the lens under the use of a spherical mesh is available by introducing more degrees of freedom in the electrode arrangement. Figure 11(a) shows a simple modification of the lens in this regard. Figure 11(b) is a further modification with a three-electrode arrangement. In these lenses, spherical aberration is corrected over a large acceptance angle of 60°. We have performed optimization on two- and three-electrode designs for different acceptance angles. The results for the spherical aberration disk size (the diameter of the blur of the image) are shown in Fig. 12. Here the distance between the object and the image is set to 500 mm. (The values can be reduced in proportion to the system size.) The three-electrode spherical mesh lens gives a significant improvement of the focusing capability of the two-electrode one. The reduction of the spherical aberration in the considered modification is around 40%, taking the difference in magnification into account.

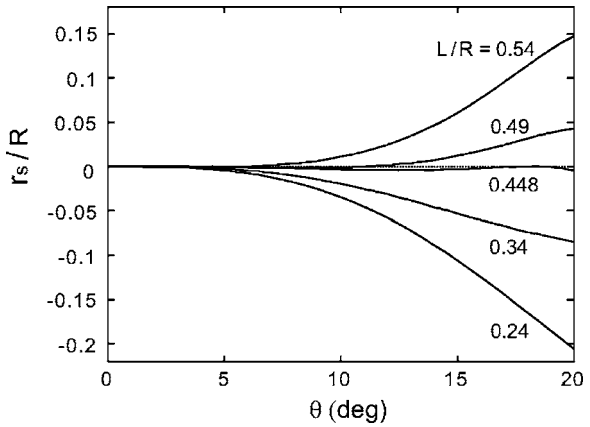

FIG. 10. Spherical aberration behavior of the mesh lens shown in Fig. 9. The spherical aberration r_s relative to the radius R of the lens is shown. Some variations of the electrode length L shown in Fig. 9 are considered. The voltage on the second electrode is adjusted to give the Gaussian image plane at the same position.

One can consider a lens design with four or more electrodes to further reduce spherical aberration. However, the reduction in this approach seems to be small, and it is difficult to realize acceptance angles larger than around 70° when using a spherical mesh. Thus, in the following section, we consider the use of an ellipsoidal mesh to obtain larger acceptance angles in deceleration lenses.

IV. DECELERATION AND FOCUSING OF WIDE-ANGLE BEAMS USING AN ELLIPSOIDAL MESH

The preceding section has shown that practical realization of focusing fields such as suggested in Sec. II B is possible using a spherical mesh and a few electrodes. Now, for further enhancement of the capability of collecting and focusing charged particles, let us consider the use of an ellipsoidal mesh, instead of a spherical mesh, following Sec. II C. Optimization of the ellipsoidal shape parameter γ, together with that of the electrode arrangement, was performed to realize fine focusing over wide acceptance angles.

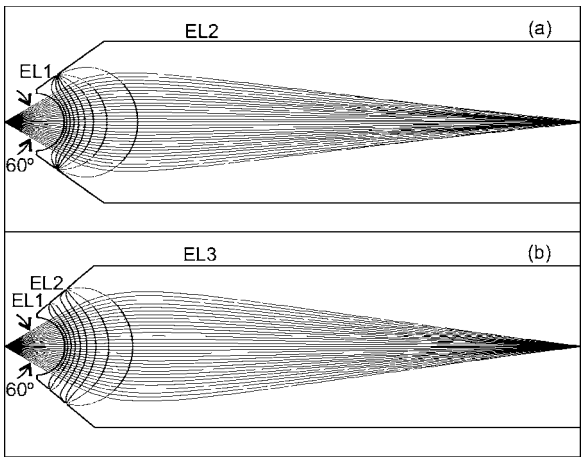

FIG. 11. Comparison between (a) two- and (b) three-electrode deceleration lenses with a spherical mesh. Equipotential lines and electron trajectories with initial angles up to ±30° are shown. The three-electrode arrangement provides good regulation of the electrostatic field.

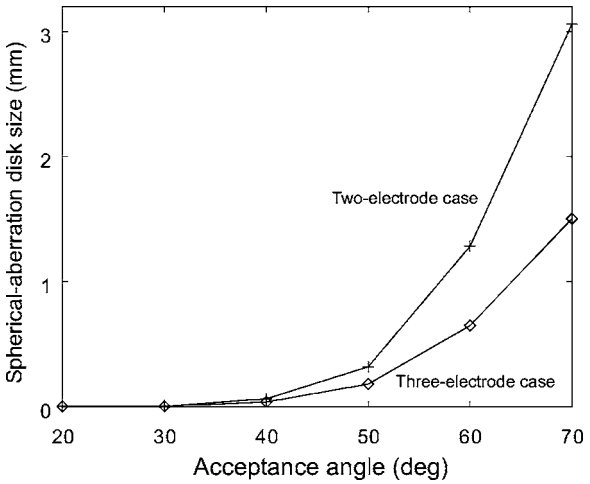

FIG. 12. Results of optimization of the electrode conditions of two- and three-electrode deceleration lenses with a spherical mesh. The values of the aberration disk size (the diameter of the blur of the image) obtained for various acceptance angles are shown. The distance between the object and the image is 500 mm.

Figure 13 shows an optimization result for a three-electrode deceleration lens with an ellipsoidal mesh. Here, spherical aberration is finely corrected over a wide acceptance angle of 100°. The first electrode EL1 and the mesh are set at ground potential and decelerating voltages V_2 and V_3 are applied to the electrodes EL2 and EL3. The deceleration ratio of the lens is around 0.18. The beam divergence angle at the image plane is around 23° (which is around the same degree as in the einzel-type mesh lens proposed in Ref. [15]). The focusing position can be well controlled in the lens; shifting the focusing position results in changing the output beam divergence angle.

The value of the ellipsoidal-shape parameter for the lens shown in Fig. 13 is $\gamma=1.50$. Note that the γ value for minimum spherical aberration, which is somewhat dependent on the electrode arrangement and the focusing position, is much larger than the one indicated in Sec. II C. This is a consequence from the fact that a single mesh is used in the considered lens design, while two ellipsoidal boundaries are sup-

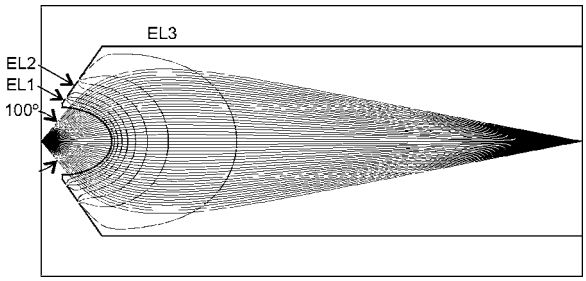

FIG. 13. A three-electrode deceleration lens with an ellipsoidal mesh. Equipotential lines and electron trajectories with initial angles up to ±50° are shown. The ellipsoidal-shape parameter is $\gamma=1.50$.

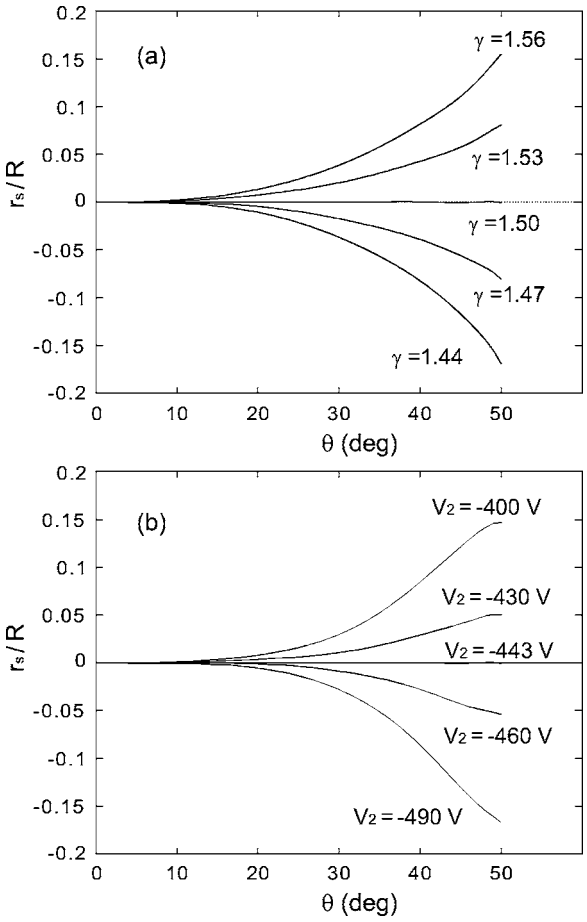

FIG. 14. Spherical aberration behavior of the wide-angle deceleration lens for a variation of (a) the ellipsoidal-shape parameter γ and (b) the voltage V_2 on the second electrode EL2. The spherical aberration r_s relative to the radius R of the cylinder of the lens is shown. It is seen that spherical aberration is very small for $\gamma=1.50$ (the case in Fig. 13). Some variations of γ and V_2 from this focusing condition are considered. The values of V_2 are shown for the case where the initial electron energy is 1 keV. The voltage on the third electrode EL3 is adjusted to give the Gaussian image plane at the same position.

posed in Sec. II C. It should also be noted that the γ value here is significantly smaller than the one ($\gamma=1.73$) obtained for the einzel-type mesh lens in Ref. [15].

In Fig. 14(a), some variations of γ from the focusing condition in Fig. 13 are considered. While increasing γ (decreasing γ) gives a shift of the image position to smaller z (larger z), we fixed the Gaussian image plane at the same position by adjusting the voltage V_3. As is shown, the parameter γ provides fine control of the degree and sign of spherical aberration. In Fig. 14(b), it is shown that the spherical aberration can be well controlled with the voltage V_2. Increasing the length of the first electrode EL1 along the slope results in producing or increasing negative spherical aberration, similar to Fig. 10. The length parameters of the electrodes EL1 and EL2, as well as the ellipsoidal-shape parameter, play an important role for fine correction of spherical aberration.

It should be noted that in the wide-angle mesh lens, the beam-divergence angle is considerably reduced at the image

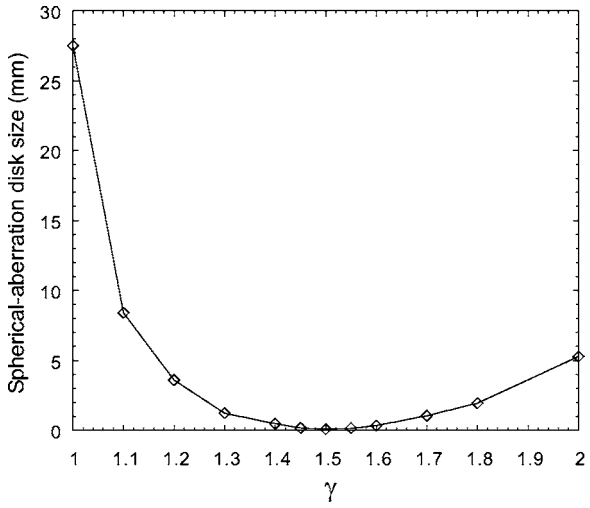

FIG. 15. Results of optimization of the electrode conditions of the three-electrode deceleration lens for various values of γ. The distance between the object and the image is 500 mm.

plane, but it is still somewhat large. Thus, a great care should be taken when considering a combination of a usual lens with the mesh lens. Figure 14 suggests that we give the wide-angle mesh lens with some degree of negative spherical aberration to cancel positive spherical aberration of an additional lens.

For various values of γ, we performed optimization of the electrode conditions. The results for the spherical aberration disk size (the diameter of the blur of the image) are shown in Fig. 15. Starting from the spherical mesh case $\gamma=1$, the spherical aberration rapidly decreases with increasing γ, and it then becomes very small at around $\gamma=1.50$, around which the aberration disk size is less than 0.1 mm. The curve in Fig. 15 has a broad minimum with values less than 1 mm between around $\gamma=1.35$ and 1.65.

Finally, we mention that it is possible to further increase the acceptance angle of the mesh lens by modifying the electrode arrangement and the mesh shape. Figure 16 shows a three-electrode deceleration lens with an acceptance angle of 120°. Here, a mesh surface larger than half of an ellipsoid is used, similarly to Fig. 8(b). The γ value used here is around the same as the γ in Fig. 13. The deceleration ratio of the lens is around 0.19. The output beam divergence angle is around 27°.

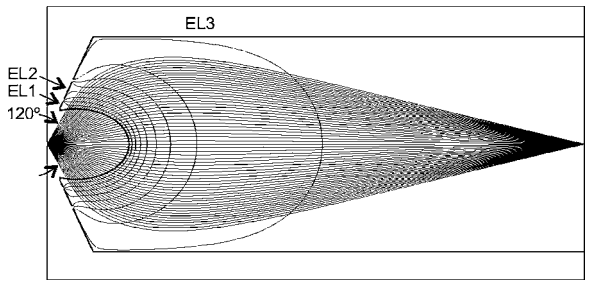

FIG. 16. A three-electrode deceleration lens with an acceptance angle of 120°. Equipotential lines and electron trajectories with initial angles up to ±60° are shown.

V. DISCUSSION AND CONCLUSION

Considerations on beam focusing using simple solutions of Laplace equation have shown some interesting features. A fundamental feature is that a spherically symmetric deceleration field provides much better focusing than ordinary deceleration lenses. Beam focusing over a wide divergence angle of 100° was shown to be possible in a situation where the deceleration ratio E_f/E_i is 0.01, which may be appropriate for beams with high energies of around 10 keV. However, large spherical aberration is produced when the deceleration ratio E_f/E_i is set to a relatively large value, around 0.1. In this situation, two essentially different deformations of the spherically symmetric field were considered. It was indicated here that a deformation of the field under a spherical boundary condition allows us to correct spherical aberration over wide acceptance angles up to around 80°. A similar consideration can be found in Ref. [14]; here, beam focusing over a large acceptance angle of 60° was shown to be possible in a situation where a focusing field of acceleration follows an entrance field. Note that the present scheme for focusing wide-angle beams is not based on the use of such a focusing field. Furthermore, it was shown that an ellipsoidal deformation of the spherically symmetric field enables correction of spherical aberration over wide-acceptance angles up to around 120°.

We demonstrated that practical realizations of such fields are possible using a few electrodes and a curved mesh. The simplest case is the equidiameter two-cylinder lens with a spherical mesh, which allows an acceptance angle of around 40°. Appropriate electrode arrangements enable realizing larger acceptance angles up to around 60°, when using a spherical mesh. A good focusing capability can be realized by a three-electrode arrangement (while the use of more electrodes can provide somewhat better focusing). The diameter of the blur of the image obtained in the three-electrode deceleration lens is around 0.7 mm when the distance between the object and the image is 500 mm. This value is of the same order as in the einzel-type spherical mesh lens proposed in Ref. [14]. A deceleration lens may be arranged behind the einzel-type spherical mesh lens. However, in this case, it is difficult to provide good focusing, as deceleration lenses in general have large spherical aberration. The decelerating spherical mesh lens has an advantage in this respect.

For realization of larger acceptance angles, we considered a three-electrode deceleration lens with an ellipsoid mesh. It was shown here that spherical aberration can be finely corrected over a wide acceptance angle of 100°. The diameter of the blur disk obtained in this lens is around 0.08 mm when the distance between the object and the image is 500 mm. The complete correction of the spherical aberration is possible by using the optimization procedure presented in the previous paper [15]. The ellipsoidal mesh lens not only provides fine focusing but also allows generation and fine control of negative spherical aberration. This feature is important because it in turn allows cancellation of positive spherical aberration when we arrange an additional lens behind the mesh lens. The dependence of the image blur on the ellipsoidal-shape parameter γ in the considered mesh lens shows a curve with a broad minimum around $\gamma=1.50$ (the blur of the image is reasonably small even at $\gamma=1.40$). Thus the mesh lens has a high tolerance for γ variation at some acceptable focusing level. It should be noted that the γ in the minimum-blur condition is significantly smaller than the one ($\gamma=1.73$) obtained for the einzel-type ellipsoidal mesh lens in Ref. [15]. For the fabrication of an ellipsoidal mesh and, in view of the electron transmission through the mesh, a mesh shape with smaller γ would be better. We have also demonstrated that in a three-electrode ellipsoidal-mesh lens, the use of a mesh surface larger than half of an ellipsoid allows us to correct spherical aberration over a wide acceptance angle of 120°. The fabrication and alignment of such a mesh is, however, not easy, and thus, the wide-angle mesh lens with an acceptance angle of less than around 100° would be better for practical realization; an acceptance angle of larger than around 90° is very fascinating for, e.g., electronic structure analysis, stereo atomscopy, and depth profile analysis.

The wide-angle lens proposed in this paper, as well as the one proposed in the previous paper [15], can serve as a powerful basis for simultaneous angular distribution measurement of charged particles. The remarkable difference between the two is that the wide-angle lens in this paper not only provides focusing of a wide-angle beam, but also, simultaneously, achieves deceleration of the beam. This lens capability would be especially important for realizing wide acceptance angles in high-energy XPS and related techniques.

[1] H. Daimon, Rev. Sci. Instrum. **59**, 545 (1988).
[2] H. Daimon and S. Ino, J. Vac. Soc. Jpn. **31**, 954 (1988).
[3] H. Daimon and S. Ino, Rev. Sci. Instrum. **61**, 57 (1990).
[4] H. Nishimoto, H. Daimon, S. Suga, Y. Tezuka, S. Ino, I. Kato, F. Zenitani, and H. Soezima, Rev. Sci. Instrum. **64**, 2857 (1993).
[5] T. Okuda, H. Daimon, M. Kotsugi, K. Nakatsuji, M. Fujikawa, S. Suga, Y. Tezuka, S. Shin, M. Kasai, and Y. Tokura, J. Electron Spectrosc. Relat. Phenom. **88–91**, 473 (1998).
[6] M. Kotsugi, H. Daimon, K. Nakatsuji, T. Okuda, T. Furuhata, M. Fujikawa, H. Takagi, Y. Tezuka, S. Shin, K. Kitahama, T. Kawai, and S. Suga, J. Electron Spectrosc. Relat. Phenom. **88–91**, 489 (1998).
[7] F. Matsui, Y. Hori, H. Miyata, N. Suganuma, H. Daimon, H. Totsuka, K. Ogawa, T. Furukubo, and H. Namba, Appl. Phys. Lett. **81**, 2556 (2002).
[8] F. Matsui, H. Miyata, O. Rader, Y. Hamada, Y. Nakamura, K. Nakanishi, K. Ogawa, H. Namba, and H. Daimon, Phys. Rev. B **72**, 195417 (2005).
[9] H. Daimon, Phys. Rev. Lett. **86**, 2034 (2001).
[10] F. Matsui, H. Daimon, F. Z. Guo, and T. Matsushita, Appl. Phys. Lett. **85**, 3737 (2004).

[11] F. Z. Guo, T. Matsushita, K. Kobayashi, F. Matsui, Y. Kato, H. Daimon, M. Koyano, Y. Yamamura, T. Tsuji, and Y. Saitoh, J. Appl. Phys. **99**, 024907 (2006).
[12] O. Scherzer, Optik (Stuttgart) **2**, 114 (1947).
[13] A. A. van Gorkum, J. Vac. Sci. Technol. B **1**, 1312 (1983).
[14] M. Kato and T. Sekine, J. Vac. Sci. Technol. B **13**, 2255 (1995).
[15] H. Matsuda, H. Daimon, M. Kato, and M. Kudo, Phys. Rev. E **71**, 066503 (2005).
[16] A. Sekiyama, T. Iwasaki, K. Matsuda, Y. Saitoh, Y. Onuki, and S. Suga, Nature (London) **403**, 396 (2000).
[17] V. Formoso, A. Filipponi, A. Di Cicco, G. Chiarello, R. Felici, and A. Santaniello, Phys. Rev. B **61**, 1871 (2000).
[18] S. Diplas, J. F. Watts, S. A. Morton, G. Beamson, P. Tsakiropoulos, D. T. Clark, and J. E. Castle, J. Electron Spectrosc. Relat. Phenom. **113**, 153 (2001).
[19] H. Piao, N. S. Mclntyre, G. Beamson, M.-L. Abel, and J. F. Watts, J. Electron Spectrosc. Relat. Phenom. **125**, 35 (2002).
[20] K. Kobayashi, M. Yabashi, Y. Takata, T. Tokushima, S. Shin, K. Tamasaku, D. Miwa, T. Ishikawa, H. Nohira, T. Hattori, Y. Sugita, O. Nakatsuka, A. Sakai, and S. Zaima, Appl. Phys. Lett. **83**, 1005 (2003).
[21] G. Beamson, S. R. Haines, N. Moslemzadeh, P. Tsakiropoulos, J. F. Watts, P. Weightman, and K. Williams, J. Electron Spectrosc. Relat. Phenom. **142**, 151 (2005).
[22] L. H. Pan, T. E. Sullivan, V. J. Peridier, P. H. Cutler, and N. M. Miskovsky, Appl. Phys. Lett. **65**, 2151 (1994).
[23] S. Patil, A. V. Kulkami, and C. V. Dharmadhikari, J. Appl. Phys. **88**, 6940 (2000).